Implementation of an Impedance-Matched Λ System by Dressed-State Engineering

Kazuki Koshino,[1] Kunihiro Inomata,[2] Tsuyoshi Yamamoto,[2,3] and Yasunobu Nakamura[2,4]

[1]*College of Liberal Arts and Sciences, Tokyo Medical and Dental University, Ichikawa, Chiba 272-0827, Japan*
[2]*RIKEN Center for Emergent Matter Science (CEMS), 2-1 Hirosawa, Wako, Saitama 351-0198, Japan*
[3]*Smart Energy Research Laboratories, NEC Corporation, Tsukuba, Ibaraki 305-8501, Japan*
[4]*Research Center for Advanced Science and Technology (RCAST), The University of Tokyo, Meguro-ku, Tokyo 153-8904, Japan*

(Received 16 June 2013; published 9 October 2013)

In one-dimensional optical setups, light-matter interaction is drastically enhanced by the interference between the incident and scattered fields. Particularly, in the impedance-matched Λ-type three-level systems, a single photon deterministically induces the Raman transition and switches the electronic state of the system. Here, we show that such a Λ system can be implemented by using dressed states of a driven superconducting qubit and a resonator. The input microwave photons are perfectly absorbed and are down-converted into other frequency modes in the same waveguide. The proposed setup is applicable to the detection of single microwave photons and the swapping of the photon and matter qubits.

DOI: 10.1103/PhysRevLett.111.153601 PACS numbers: 42.50.Pq, 03.67.Lx, 85.25.Cp

In one-dimensional optical setups, radiation from a quantum emitter is guided completely to specified one-dimensional propagating modes. We can realize such setups in a variety of physical systems, such as optical cavity quantum electrodynamics (QED) systems using atoms or quantum dots [1–3] and circuit QED systems using superconducting qubits [4–6]. When we apply a field to excite the emitter through the one-dimensional mode in these setups, the incident field inevitably interferes with the field scattered by the emitter due to the low dimensionality [7]. As a result, we can realize unique optical phenomena that are not achievable in three-dimensional free space. A classical example is the complete transmission of a resonant field through a two-sided cavity, in which reflection from the cavity is forbidden due to the destructive interference between the incident field and the cavity emission in the reflection direction. Such one-dimensional optical setups in which reflection from the emitter is forbidden are called impedance matched, in analogy with properly terminated electric circuits [8,9]. Recently, perfect reflection of the incident field by a single emitter has been confirmed in both optical cavity QED and circuit QED systems [2,4]. Here, transmission is forbidden by the destructive interference occurring in the transmission direction.

In this study, we investigate a three-level Λ system interacting with a semi-infinite one-dimensional field in a reflection geometry (Fig. 1). We denote the three levels of the Λ system by $|g\rangle$, $|m\rangle$, and $|e\rangle$ from the lowest. We assume that $|m\rangle$ decays to $|g\rangle$ with a finite lifetime and therefore that the system is in $|g\rangle$ when stationary. When a single photon resonant to the $|g\rangle \to |e\rangle$ transition is input, there are three possible processes: (a) simple reflection without exciting the system, (b) elastic scattering, inducing the $|g\rangle \to |e\rangle \to |g\rangle$ transitions, and (c) inelastic scattering, inducing the $|g\rangle \to |e\rangle \to |m\rangle \to |g\rangle$ transitions. Destructive interference occurs here between processes (a) and (b). In particular, they cancel each other completely when the two decay rates from the top level $|e\rangle$ are identical ($\Gamma_{eg} = \Gamma_{em}$) and the coherence length of the input photon is sufficiently long. As a result, the input photon is down-converted deterministically, inducing the Raman transition in the system [Fig. 1(c)] [10]. This is the impedance matching in the Λ system. The charm of such impedance-matched systems is the deterministic electronic dynamics induced by single photons, which enables novel quantum technologies. Based on such Λ systems, single-photon transistors, quantum memories, and optical quantum gates have been theoretically proposed [11–16].

In superconducting qubits, we use several discrete levels formed at the bottom of the anharmonic potential as an artificial atom. We usually make the potential symmetric in order to suppress dephasing. Then, each eigenstate has a definite parity and the qubit functions as a ladder-type multilevel system. We can also make the potential asymmetric, for example, by introducing flux bias in flux qubits. The lowest three levels then function as a Λ system, which has been used to demonstrate, for example, lasing and cooling of qubits [17–19]. However, it is difficult to satisfy the impedance-matching condition, i.e., identical decay rates from the second excited state, in the Λ systems thus created.

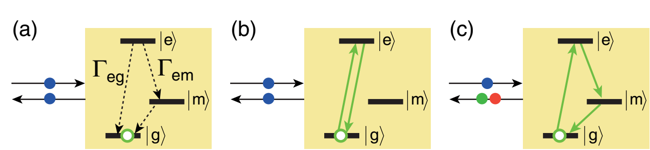

FIG. 1 (color online). Interaction between a Λ system and a photon propagating in a semi-infinite one-dimensional waveguide: (a) simple reflection, (b) elastic scattering, and (c) inelastic scattering. Γ_{ij} ($i, j = e, m, g$) denotes the radiative decay rate for the $|i\rangle \to |j\rangle$ transition.

In this study, we propose a practical scheme for implementing an impedance-matched Λ system by using dressed states of a qubit and a resonator. The schematic of the considered setup is shown in Fig. 2. A superconducting qubit is coupled to a resonator, which is further coupled to a semi-infinite waveguide (waveguide 1). Through another waveguide (waveguide 2), a drive field $E(t)$ is applied to the qubit. The qubit functions as a two-level system ($|0\rangle$ and $|1\rangle$). Setting $\hbar = v = 1$, where v is the microwave velocity in the waveguides, the Hamiltonian of the system is

$$\mathcal{H}(t) = \mathcal{H}_{\rm sys}(t) + \mathcal{H}_{\rm damp}, \tag{1}$$

$$\mathcal{H}_{\rm sys}(t) = \omega_q \sigma^\dagger \sigma + \omega_r a^\dagger a + g(\sigma^\dagger a + a^\dagger \sigma) + \sqrt{\gamma}[E(t)\sigma^\dagger + E^*(t)\sigma], \tag{2}$$

$$\mathcal{H}_{\rm damp} = \int dk[k b_k^\dagger b_k + \sqrt{\kappa/2\pi}(a^\dagger b_k + b_k^\dagger a)] + \int dk[k c_k^\dagger c_k + \sqrt{\gamma/2\pi}(\sigma^\dagger c_k + c_k^\dagger \sigma)]. \tag{3}$$

The meanings of the operators are as follows: σ (a) is the annihilation operator of the qubit (resonator), and b_k (c_k) is the photon annihilation operator in waveguide 1 (2) with wave number k. The meanings of the parameters are as follows: ω_q (ω_r) is the resonance frequency of the qubit (resonator), g is the qubit-resonator coupling, and κ (γ) is the decay rate of the resonator (qubit) into waveguide 1 (2). For simplicity, γ is assumed to include the nonradiative decay of the qubit. We consider the case in which the qubit and the resonator are highly detuned ($|\omega_r - \omega_q| \gg g$) and are coupled dispersively. The drive field is monochromatic $E(t) = Ee^{-i\omega_d t}$ and is close to the resonance of the qubit.

By switching to the frame rotating at the drive frequency ω_d, the Hamiltonian becomes static. Then, $\mathcal{H}_{\rm sys} = (\omega_q - \omega_d)\sigma^\dagger\sigma + (\omega_r - \omega_d)a^\dagger a + g(\sigma^\dagger a + a^\dagger \sigma) + \sqrt{\gamma}(E\sigma^\dagger + E^*\sigma)]$. $\mathcal{H}_{\rm damp}$ remains unchanged, except that the photon frequency is measured from ω_d. We denote the eigenstates of $\mathcal{H}_{\rm sys}$ by $|\tilde{j}\rangle$ and their energies by $\tilde{\omega}_j$ ($j = 1, 2, \dots$) from the lowest. Using the qubit-resonator eigenstates, the Hamiltonian is rewritten as

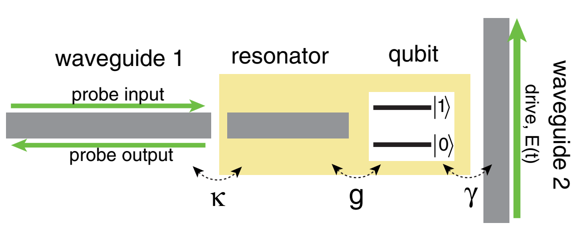

FIG. 2 (color online). Schematic of the considered setup. A qubit is coupled dispersively to a resonator, which is further coupled to a semi-infinite waveguide (waveguide 1). The qubit is driven by a microwave field propagating along another waveguide (waveguide 2).

$$\mathcal{H} = \mathcal{H}_{\rm sys} + \mathcal{H}_{\rm damp}, \tag{4}$$

$$\mathcal{H}_{\rm sys} = \sum_j \tilde{\omega}_j \tilde{\sigma}_{jj}, \tag{5}$$

$$\mathcal{H}_{\rm damp} = \int dk\Big[k b_k^\dagger b_k + \sum_{i,j}\sqrt{\tilde{\kappa}_{ij}/2\pi}(\tilde{\sigma}_{ij} b_k + b_k^\dagger \tilde{\sigma}_{ji})\Big] + \int dk\Big[k c_k^\dagger c_k + \sum_{i,j}\sqrt{\tilde{\gamma}_{ij}/2\pi}(\tilde{\sigma}_{ij} c_k + c_k^\dagger \tilde{\sigma}_{ji})\Big], \tag{6}$$

where $\tilde{\sigma}_{ij} = |\tilde{i}\rangle\langle\tilde{j}|$ and $\tilde{\kappa}_{ij}$ ($\tilde{\gamma}_{ij}$) is the radiative decay rate into waveguide 1 (2) for the $|\tilde{i}\rangle \longrightarrow |\tilde{j}\rangle$ transition. $\tilde{\kappa}_{ij}$ and $\tilde{\gamma}_{ij}$ are, respectively, given by

$$\tilde{\kappa}_{ij} = \kappa|\langle\tilde{i}|a^\dagger|\tilde{j}\rangle|^2, \tag{7}$$

$$\tilde{\gamma}_{ij} = \gamma|\langle\tilde{i}|\sigma^\dagger|\tilde{j}\rangle|^2. \tag{8}$$

For $g = E = 0$, the eigenstates of $\mathcal{H}_{\rm sys}$ are simply the product Fock states of the qubit and the resonator $|m, n\rangle = |m\rangle_q|n\rangle_r$ ($m = 0$, 1 and $n = 0, 1, \dots$). The qubit-resonator coupling g mixes these states only slightly due to the large detuning and brings about dispersive level shifts. Within the second-order perturbation, the eigenenergies are given by

$$\omega_{|0,n\rangle} = n(\omega_r - \omega_d + \chi), \tag{9}$$

$$\omega_{|1,n\rangle} = \omega_q - \omega_d - \chi + n(\omega_r - \omega_d - \chi), \tag{10}$$

where $\chi = g^2/(\omega_r - \omega_q)$. In this study, we investigate the case in which a weak probe field is input from waveguide 1. Therefore, only the four lowest levels ($|0, 0\rangle$, $|1, 0\rangle$, $|0, 1\rangle$, and $|1, 1\rangle$) are relevant. Their energy diagrams are shown in Fig. 3 for $E = 0$. Because of the dispersive level shifts, with the proper choice of the drive frequency ω_d ($\omega_q - 3\chi < \omega_d < \omega_q - \chi$), the level structure becomes nested, i.e., $\omega_{|0,0\rangle} < \omega_{|1,0\rangle} < \omega_{|1,1\rangle} < \omega_{|0,1\rangle}$ [Fig. 3(a)]. When ω_d is out of this range, the level structure becomes un-nested [Fig. 3(b)]. We refer to the former (latter) case as the nesting (un-nesting) regime hereafter.

Next, we discuss the effects of driving. The drive field mixes the two lower (higher) levels in Fig. 3 to form dressed states $|\tilde{1}\rangle$ and $|\tilde{2}\rangle$ ($|\tilde{3}\rangle$ and $|\tilde{4}\rangle$). Therefore, neglecting the slight mixing originating in the dispersive coupling, dressed states are roughly written as $|\tilde{1}\rangle \simeq \cos\alpha|0, 0\rangle - \sin\alpha|1, 0\rangle$, $|\tilde{2}\rangle \simeq \sin\alpha|0, 0\rangle + \cos\alpha|1, 0\rangle$, $|\tilde{3}\rangle \simeq \cos\beta|0, 1\rangle - \sin\beta|1, 1\rangle$, and $|\tilde{4}\rangle \simeq \sin\beta|0, 1\rangle + \cos\beta|1, 1\rangle$, where α and β depend on the frequency ω_d and the power $|E|^2$ of the drive field. From Eq. (7), the radiative decay rates $\tilde{\kappa}_{ij}$ into waveguide 1 are given by $\tilde{\kappa}_{31} \simeq \tilde{\kappa}_{42} \simeq \kappa\cos^2(\alpha - \beta)$, and $\tilde{\kappa}_{32} \simeq \tilde{\kappa}_{41} \simeq \kappa\sin^2(\alpha - \beta)$, and others vanish. For weak drive, $(\alpha, \beta) \simeq (0, \pi/2)$, and accordingly, $\tilde{\kappa}_{32} \simeq \tilde{\kappa}_{41} \simeq \kappa$ in the nesting regime [Fig. 3(a)], whereas $(\alpha, \beta) \simeq (0, 0)$,

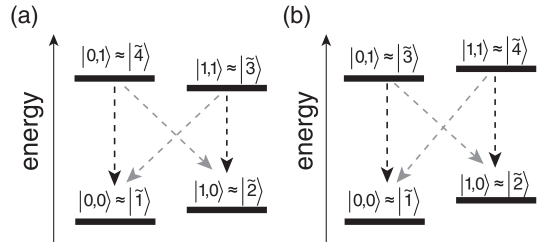

FIG. 3. Structure of the four lowest levels of the qubit-resonator system for $E = 0$: (a) Nesting and (b) un-nesting regimes. The nesting regime is realized when the drive frequency satisfies $\omega_q - 3\chi < \omega_d < \omega_q - \chi$. Arrows indicate the direction of the cavity decay. Oblique decay paths (gray arrows) are generated by the drive field ($E \neq 0$).

and accordingly, $\tilde{\kappa}_{31} \simeq \tilde{\kappa}_{42} \simeq \kappa$ in the un-nesting regime [Fig. 3(b)]. In contrast, for strong drive, where the Rabi splittings overwhelm the dispersive level shifts, $(\alpha, \beta) \simeq (\pi/4, \pi/4)$ and therefore $\tilde{\kappa}_{31} \simeq \tilde{\kappa}_{42} \simeq \kappa$ in both nesting and un-nesting regimes. In Figs. 4(a) and 4(b), $\tilde{\kappa}_{31}$, $\tilde{\kappa}_{32}$, $\tilde{\kappa}_{41}$, and $\tilde{\kappa}_{42}$ are evaluated rigorously from Eq. (7), using the Rabi frequency $\Omega_R = \sqrt{\gamma}|E|$ as a measure of the drive power. We observe that $\tilde{\kappa}_{31} \simeq \tilde{\kappa}_{42}$ and $\tilde{\kappa}_{32} \simeq \tilde{\kappa}_{41}$ at any drive power in accordance with the above discussion. Remarkably, inversion of these decay rates occurs in the nesting regime [Fig. 4(a)], and the two radiative decay rates from $|\tilde{3}\rangle$ or $|\tilde{4}\rangle$ become identical with the proper choice of the drive power ($\Omega_R/2\pi \approx 19$ MHz). At this drive power, the qubit-resonator system functions as an impedance-matched Λ system, with $|g\rangle = |\tilde{1}\rangle$, $|m\rangle = |\tilde{2}\rangle$, and $|e\rangle = |\tilde{3}\rangle$ or $|\tilde{4}\rangle$.

In this work, we set the drive frequency close to the lower edge of the nesting regime, i.e., $\omega_d \approx \omega_q - 3\chi$. Then, the two upper bare states in Fig. 3 are nearly degenerate and are mixed strongly by the drive, whereas the two lower bare states remain almost unmixed due to the large detuning about 2χ: $|g\rangle \simeq |0, 0\rangle$ (qubit ground state) and $|m\rangle \simeq |0, 1\rangle$ (qubit excited state). Therefore, the decay rate Γ_{mg} is of the qubit origin and $\Gamma_{mg} \simeq \gamma$, while Γ_{eg} and Γ_{em} are of the cavity origin and $\Gamma_{eg} = \Gamma_{em} \simeq \kappa/2$. If the drive frequency is closer to the center of the nesting regime, i.e., $\omega_d \approx \omega_q - 2\chi$, a stronger drive is required to generate the dressed states, since both the lower and upper states have large detunings about χ. When $\omega_d/2\pi = 4.9$ GHz, for example, the impedance-matching condition is satisfied at $\Omega_R/2\pi \approx 26$ MHz.

In the following, we analyze the microwave response of this qubit-resonator system to a probe field applied through waveguide 1. From the Hamiltonian of Eq. (4), the Heisenberg equation for $\tilde{\sigma}_{ij}$ is

$$\frac{d}{dt}\tilde{\sigma}_{ij} = i\tilde{\omega}_{ij}\tilde{\sigma}_{ij} - (\xi_{ij}^{\kappa} + \xi_{ij}^{\gamma})/2 + i[\zeta_{ij}^{\kappa\dagger} b_{\rm in}(t) + \zeta_{ij}^{\gamma\dagger} c_{\rm in}(t)] - i[b_{\rm in}^{\dagger}(t)\zeta_{ji}^{\kappa} + c_{\rm in}^{\dagger}(t)\zeta_{ji}^{\gamma}], \tag{11}$$

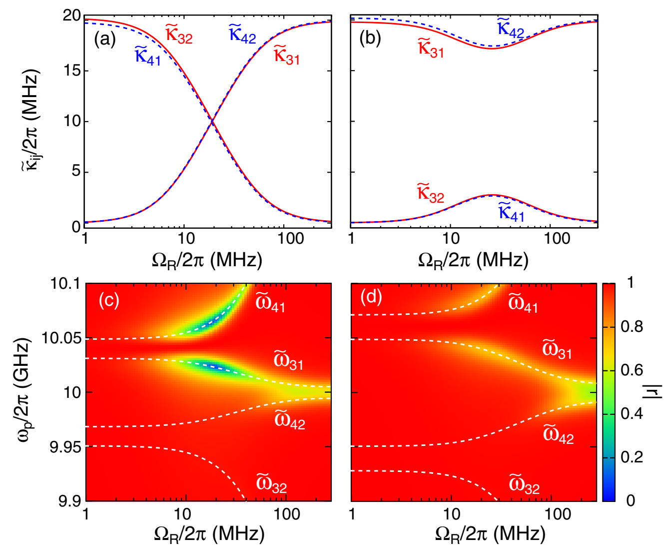

FIG. 4 (color online). (a) Dependences of $\tilde{\kappa}_{31}$, $\tilde{\kappa}_{32}$, $\tilde{\kappa}_{41}$, and $\tilde{\kappa}_{42}$ on the drive power. The drive frequency is in the nesting regime ($\omega_d/2\pi = 4.87$ GHz). The drive power is expressed in terms of the Rabi frequency $\Omega_R = \sqrt{\gamma}|E|$. The curves for $\tilde{\kappa}_{31}$ and $\tilde{\kappa}_{42}$ ($\tilde{\kappa}_{32}$ and $\tilde{\kappa}_{41}$) are mostly overlapping. (b) The same plot as (a) in the un-nesting regime ($\omega_d/2\pi = 4.83$ GHz). (c) Reflection coefficient $|r|$ as a function of the drive power and the probe frequency in the nesting regime ($\omega_d/2\pi = 4.87$ GHz). (d) Same plot as (c) in the un-nesting regime ($\omega_d/2\pi = 4.83$ GHz). In (c) and (d), the probe field is weak ($|F|^2 = 10^2$ photons/s) and is in the linear-response regime. The following parameters are assumed: $\omega_q/2\pi = 5$ GHz, $\omega_r/2\pi = 10$ GHz, $g/2\pi = 500$ MHz, $\kappa/2\pi = 20$ MHz, and $\gamma/2\pi = 0.1$ MHz.

where $S_\mu = \sum_{m,n} \sqrt{\tilde{\mu}_{mn}}\, \tilde{\sigma}_{nm}$ ($\mu = \kappa, \gamma$), $\xi_{ij}^{\mu} = \tilde{\sigma}_{ij} S_\mu^\dagger S_\mu + S_\mu^\dagger S_\mu \tilde{\sigma}_{ij} - 2S_\mu^\dagger \tilde{\sigma}_{ij} S_\mu$, and $\zeta_{ij}^{\mu} = [\tilde{\sigma}_{ji}, S_\mu]$. The input and output field operators $b_{\rm in}(t)$ and $b_{\rm out}(t)$ are connected by

$$b_{\rm out}(t) = b_{\rm in}(t) - iS_\kappa(t). \tag{12}$$

We assume that a monochromatic probe field with amplitude F and frequency ω_p is applied from waveguide 1, while no probe field is applied from waveguide 2, i.e., $\langle b_{\rm in}(t)\rangle = Fe^{-i(\omega_p - \omega_d)t}$ and $\langle c_{\rm in}(t)\rangle = 0$. Note that the probe frequency ω_p is measured from the drive frequency ω_d since we are working in the rotating frame.

We define the reflection coefficient by the ratio of output and input amplitudes, i.e., $r = \langle b_{\rm out}(t)\rangle/\langle b_{\rm in}(t)\rangle$. For a weak probe, the system exhibits linear response, and therefore r is independent of the probe power. In Figs. 4(c) and 4(d), $|r|$ is plotted as a function of the drive power and the probe frequency, together with the relevant transition frequencies between dressed states. We observe considerable attenuation of $|r|$, which results from inelastic scattering. In particular, the reflected field amplitude nearly vanishes in the nesting regime [Fig. 4(c)] as a result of the impedance matching. The conditions are that (i) the decay rates from $|\tilde{3}\rangle$ ($|\tilde{4}\rangle$) to $|\tilde{1}\rangle$ and $|\tilde{2}\rangle$ are identical [$\Omega_R/2\pi \simeq$ 19 MHz in Fig. 4(a)] and that (ii) the probe frequency is tuned to $\tilde{\omega}_{31}$ ($\tilde{\omega}_{41}$). Since level $|\tilde{2}\rangle$ is almost unoccupied for a weak probe power, no specific signal appears at $\tilde{\omega}_{32}$ or $\tilde{\omega}_{42}$. We observe in Fig. 4(d) that impedance matching never occurs in the un-nesting regime.

Although the probe amplitude vanishes, this does not imply dissipation of the probe power. Figure 5(a) plots the power spectrum density of the output field (reflected field in waveguide 1) $S(\omega) = \hbar\omega \mathrm{Re} \int_0^\infty d\tau e^{-i(\omega-\omega_d)\tau} \langle \tilde{b}_{\mathrm{out}}^\dagger(t+\tau)\tilde{b}_{\mathrm{out}}(t)\rangle/\pi$ under the impedance-matching condition. The input probe is tuned to $\tilde{\omega}_{41}(\approx 2\pi \times 10.066$ GHz). However, upon the interaction with the Λ system, the probe field is down-converted nearly completely and forms a dominant peak at $\tilde{\omega}_{42}(\approx 2\pi \times 9.977$ GHz). We define the down-conversion efficiency as the probability to detect the down-converted photons in waveguide 1, i.e., $\int_{\omega_L}^{\omega_H} d\omega(\hbar\omega)^{-1}S(\omega)/|F^2|$, where $\omega_{L,H} = \tilde{\omega}_{42} \pm 2\pi \times$ 30 MHz. Figure 5(b) plots the down-conversion efficiency. We observe that, at low probe power, most input photons are down-converted. The conversion efficiency is slightly less than unity even in the weak-probe limit, which is due to the $|\tilde{4}\rangle \to |\tilde{3}\rangle$ decay. The conversion efficiency decreases as the probe power increases. This is due to saturation of the Λ system: The bottleneck process in the down-conversion cycle $|\tilde{1}\rangle \to |\tilde{4}\rangle \to |\tilde{2}\rangle \to |\tilde{1}\rangle$ is the $|\tilde{2}\rangle \to |\tilde{1}\rangle$ decay, the rate of which is approximately γ. Therefore, when the input flux exceeds γ^{-1} ($|F|^2 \gtrsim 10^6$ photons/s), $|\tilde{2}\rangle$ is more populated than $|\tilde{1}\rangle$. Then, the probe field tuned at $\tilde{\omega}_{41}$ tends to be reflected without interacting with the Λ system. The conditions to approach the unit conversion efficiency are that (i) the $|\tilde{4}\rangle \to |\tilde{2}\rangle$ decay dominates the $|\tilde{4}\rangle \to |\tilde{3}\rangle$ decay, which requires $\kappa \gg \gamma$, and (ii) the input field does not saturate the Λ system, which requires $\gamma \gtrsim |F^2|$.

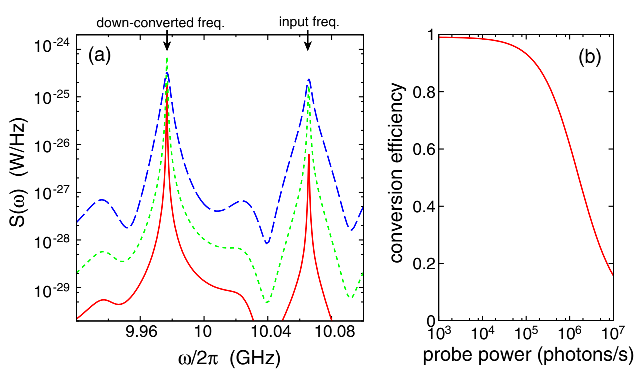

FIG. 5 (color online). (a) Power spectrum density of the output field (reflected field in waveguide 1) under the impedance-matching condition ($\omega_d/2\pi = 4.87$ GHz and $\Omega_R/2\pi \approx$ 19 MHz). The input probe frequency is tuned to $\tilde{\omega}_{41}$ ($2\pi \times 10.066$ GHz), whereas the dominant peak appears at $\tilde{\omega}_{42}$ ($2\pi \times 9.977$ GHz). The probe power $|F|^2$ is 10^5 (solid line), 10^6 (dotted line) and 10^7 (dashed line) photons/s, respectively. (b) Down-conversion efficiency as a function of the probe power.

Four final comments are in order. (i) For impedance matching, achieving the nested energy diagram [Fig. 3(a)] is essential, and therefore a large dispersive shift χ is advantageous [20]. In this regard, the systems in the so-called straddling regime are promising, in which the dispersive shift is enhanced by the presence of the second excited state of the qubit [21,22]. Numerical results are qualitatively unchanged if we extend the model in this direction. (ii) When a resonant photon with pulse length τ is input from waveguide 1, it induces the $|g\rangle \to |e\rangle \to |m\rangle$ transition nearly deterministically, provided that $\tau \gtrsim \kappa^{-1}$. For example, assuming a square pulse with $\tau = 0.33(0.67)$ μs, this probability amounts to 0.9 (0.95) for $\kappa/2\pi = 20$ MHz [10]. This deterministic Raman transition induced by single photons has wide applications [10–16]. For example, this can be used as a down-converter of single microwave photons [10]. Down-conversion of single visible or infrared photons has also been achieved as the weak-signal limit of the classical nonlinear optics [23,24]. There, a high-power pump beam propagates collinearly with the target photon in order to fulfill the phase-matching condition and to maximize the conversion efficiency. In contrast, in this work, we apply a low-power drive field which has little spatial overlap with the target photon. The large cooperativity of the qubit-resonator system assures that the target photon propagates along waveguide 1. (iii) As discussed, $|g\rangle$ and $|m\rangle$, respectively, correspond to the qubit's ground and excited states. Therefore, a single photon excites the qubit nearly deterministically. Combining this with the dispersive quantum-nondemolition readout of the qubit [25,26], we can apply this setup to the detection of single microwave photons [27–29]. A large dispersive shift is advantageous also in this regard. The principle of photon detection in Refs. [27–29] is also the impedance matching. Therefore, similar detection efficiencies are expected in both schemes after optimizing the input pulse. The practical merit of the present scheme is the small energy dissipation from the system upon detection, which would substantially reduce the backaction noise and/or the dead time of the detector. (iv) The present system functions as a SWAP gate between the photon qubit (encoded in frequency $|\tilde{\omega}_{41}\rangle$ and $|\tilde{\omega}_{42}\rangle$) and the matter qubit (encoded in $|g\rangle$ and $|m\rangle$) [12,14,15]. In other words, the Λ system memorizes the input photon qubit, and the output photon carries the initial state of the Λ system. This resembles the atomic quantum memories used in the light storage experiments [30–32]. A characteristic of the present phenomenon is the bidirectional nature of the quantum-state transfer. A practical problem would be the finite lifetime of the qubit excited state. However, we can overcome this problem by improving the qubit's lifetime [33]. Such swapping between the photon and matter qubits would be a crucial step for the realization of a scalable quantum network.

In summary, we proposed a circuit QED implementation of an impedance-matched Λ system. We considered a setup composed of a driven superconducting qubit, a resonator, and a waveguide. The four lowest eigenstates of the qubit-resonator system $|\tilde{1}\rangle$, $|\tilde{2}\rangle$, $|\tilde{3}\rangle$, and $|\tilde{4}\rangle$ are relevant in this study. With the proper choice of the drive frequency and power, two radiative decay rates from $|\tilde{3}\rangle$ or $|\tilde{4}\rangle$ become identical; the system then functions as an impedance-matched Λ system, where $|g\rangle = |\tilde{1}\rangle$, $|m\rangle = |\tilde{2}\rangle$, and $|e\rangle = |\tilde{3}\rangle$ or $|\tilde{4}\rangle$. When a probe field tuned to the $|g\rangle \rightarrow |e\rangle$ transition is applied from the waveguide, the probe field loses its coherent amplitude and is down-converted nearly completely. The present setup is applicable to the detection of single microwave photons and the swapping of the photon and matter qubits.

This work was partly supported by the Funding Program for World-Leading Innovative R&D on Science and Technology (FIRST), the Project for Developing Innovation Systems of MEXT and MEXT KAKENHI (Grants No. 21102002 and No. 25400417), SCOPE (111507004), the National Institute of Information and Communications Technology (NICT), and the Research Foundation for Opto-Science and Technology.

[1] Q. A. Turchette, C. J. Hood, W. Lange, H. Mabuchi, and H. J. Kimble, Phys. Rev. Lett. **75**, 4710 (1995).
[2] T. Aoki, A. S. Parkins, D. J. Alton, C. A. Regal, B. Dayan, E. Ostby, K. J. Vahala, and H. J. Kimble, Phys. Rev. Lett. **102**, 083601 (2009).
[3] I. Fushman, D. Englund, A. Faraon, N. Stoltz, P. Petroff, and J. Vukovic, Science **320**, 769 (2008).
[4] O. Astafiev, A. M. Zagoskin, A. A. Abdumalikov, Jr., Yu. A. Pashkin, T. Yamamoto, K. Inomata, Y. Nakamura, and J. S. Tsai, Science **327**, 840 (2010).
[5] I.-C. Hoi, C. M. Wilson, G. Johansson, T. Palomaki, B. Peropadre, and P. Delsing, Phys. Rev. Lett. **107**, 073601 (2011).
[6] C. Lang, C. Eichler, L. Steffen, J. M. Fink, M. J. Woolley, A. Blais, and A. Wallraff, Nat. Phys. **9**, 345 (2013).
[7] M. J. Collett and C. W. Gardiner, Phys. Rev. A **30**, 1386 (1984).
[8] M. Afzelius and C. Simon, Phys. Rev. A **82**, 022310 (2010).
[9] J. T. Hill, A. H. Safavi-Naeini, J. Chan, and O. Painter, Nat. Commun. **3**, 1196 (2012).
[10] K. Koshino, Phys. Rev. A **79**, 013804 (2009).
[11] D. E. Chang, A. S. Sørensen, E. A. Demler, and M. D. Lukin, Nat. Phys. **3**, 807 (2007).
[12] K. Koshino, S. Ishizaka, and Y. Nakamura, Phys. Rev. A **82**, 010301(R) (2010).
[13] D. Witthaut and A. S. Sørensen, New J. Phys. **12**, 043052 (2010).
[14] J. Gea-Banacloche and L. M. Pedrotti, Phys. Rev. A **83**, 042333 (2011).
[15] J. Gea-Banacloche and L. M. Pedrotti, Phys. Rev. A **86**, 052311 (2012).
[16] A. Kalachev and O. Kocharovskaya, Phys. Rev. A **83**, 053849 (2011).
[17] S. O. Valenzuela, W. D. Oliver, D. M. Berns, K. K. Berggren, L. S. Levitov, and T. P. Orlando, Science **314**, 1589 (2006).
[18] M. Grajcar, S. H. W. van der Ploeg, A. Izmalkov, E. Il'ichev, H.-G. Meyer, A. Fedorov, A. Shnirman, and G. Schön, Nat. Phys. **4**, 612 (2008).
[19] J. Q. You and F. Nori, Nature (London) **474**, 589 (2011).
[20] P. Forn-Díaz, J. Lisenfeld, D. Marcos, J. J. García-Ripoll, E. Solano, C. J. P. M. Harmans, and J. E. Mooij, Phys. Rev. Lett. **105**, 237001 (2010).
[21] J. Koch, T. M. Yu, J. Gambetta, A. A. Houck, D. I. Schuster, J. Majer, A. Blais, M. H. Devoret, S. M. Girvin, and R. J. Schoelkopf, Phys. Rev. A **76**, 042319 (2007).
[22] K. Inomata, T. Yamamoto, P.-M. Billangeon, Y. Nakamura, and J. S. Tsai, Phys. Rev. B **86**, 140508(R) (2012).
[23] R. Ikuta, Y. Kusaka, T. Kitano, H. Kato, T. Yamamoto, M. Koashi, and N. Imoto, Nat. Commun. **2**, 1544 (2011).
[24] J. S. Pelc, L. Yu, K. De Greve, P. L. McMahon, C. M. Natarajan, V. Esfandyarpour, S. Maier, C. Schneider, M. Kamp, S. Höfling, R. H. Hadfield, A. Forchel, Y. Yamamoto, and M. M. Fejer, Opt. Express **20**, 27 510 (2012).
[25] F. Mallet, F. R. Ong, A. Palacios-Laloy, F. Nguyen, P. Bertet, D. Vion, and D. Esteve, Nat. Phys. **5**, 791 (2009).
[26] R. Vijay, D. H. Slichter, and I. Siddiqi, Phys. Rev. Lett. **106**, 110502 (2011).
[27] Y.-F. Chen, D. Hover, S. Sendelbach, L. Maurer, S. T. Merkel, E. J. Pritchett, F. K. Wilhelm, and R. McDermott, Phys. Rev. Lett. **107**, 217401 (2011).
[28] B. Peropadre, G. Romero, G. Johansson, C. M. Wilson, E. Solano, and J. J. García-Ripoll, Phys. Rev. A **84**, 063834 (2011).
[29] A. Poudel, R. McDermott, and M. G. Vavilov, Phys. Rev. B **86**, 174506 (2012).
[30] H. P. Specht, C. Nölleke, A. Reiserer, M. Uphoff, E. Figueroa, S. Ritter, and G. Rempe, Nature (London) **473**, 190 (2011).
[31] Y. O. Dudin, L. Li, and A. Kuzmich, Phys. Rev. A **87**, 031801 (2013).
[32] G. Heinze, C. Hubrich, and T. Halfmann, Phys. Rev. Lett. **111**, 033601 (2013).
[33] C. Rigetti, J. M. Gambetta, S. Poletto, B. L. T. Plourde, J. M. Chow, A. D. Córcoles, J. A. Smolin, S. T. Merkel, J. R. Rozen, G. A. Keefe, M. B. Rothwell, M. B. Ketchen, and M. Steffen, Phys. Rev. B **86**, 100506(R) (2012).